processes

MDPI

Article

Analysis of Fluid Flow in a Radial Centrifugal Pump

Jan Černý and Martin Polák *

Department of Mechanical Engineering, Faculty of Engineering, Czech University of Life Sciences Prague, Kamýcká 129, 16521 Prague, Czech Republic
* Correspondence: karel@tf.czu.cz

Abstract: The paper presents a validation of the results of a numerical model of radial centrifugal pump flow using a PIV (Particle Image Velocimetry) experimental method. For this purpose, a 3D model of the pump was created in Inventor, which was then used to design a numerical flow model in Ansys in the CFX module. The performance characteristics of the same pump were measured on an experimental test circuit, and vector maps of the flow in the suction pipe were obtained using the PIV method. The results of the experiment—vector fields of fluid velocity distribution in a suction pipe—were then compared with the outputs of the numerical Ansys model, namely the streamlines and pressure distributions. This comparison demonstrated that the numerical model is most consistent with reality if the input variables are the pressure in front of the pump and the mass flow behind the pump. In this case, the model can determine the pressure at the pump inlet with a deviation of 1% to 10% and create streamlines in the suction pipe corresponding to the results of PIV measurements.

Keywords: Particle Image Velocimetry (PIV); ANSYS; centrifugal pump; performance characteristic

check for updates

Citation: Černý, J.; Polák, M. Analysis of Fluid Flow in a Radial Centrifugal Pump. *Processes* **2023**, *11*, 448. https://doi.org/10.3390/pr11020448

Academic Editors: Udo Fritsching and David Herak

Received: 21 December 2022
Revised: 20 January 2023
Accepted: 27 January 2023
Published: 2 February 2023

Copyright: © 2023 by the authors. Licensee MDPI, Basel, Switzerland. This article is an open access article distributed under the terms and conditions of the Creative Commons Attribution (CC BY) license (https://creativecommons.org/licenses/by/4.0/).

1. Introduction

As modern technologies advance, the design and innovation of machine parts is increasingly transferred to the virtual environment. The programs Catia, Inventor, SolidEdge, SolidWorks, NX cad, CFturbo, and many others have been used recently for this purpose [1]. The Ansys, TCAE, FlexSim, AutoCAD CFD, and other programs are used to simulate fluid flow. They are used to verify the functionality or innovation of components [2,3]. These simulation programs provide a clear picture of the pump flow without the need for experimental measurements on the actual machine. They can also provide information on the pump's limit state characteristics. For example, Sankar [4] used Ansys to study the impact of change in the number of impeller blades and the size of their outlet angle on the efficiency and head of the pump. Many studies have focused on the flow and pressure distribution in the pump, specifically in the impeller and spiral casing area. For example, Meng et al. [5] used a radial centrifugal pump for this purpose. He created a mesh in Ansys CFX, used ICEM software for the calculation, and then verified the results of the numerical model using an identical real pump on a test circuit. For this purpose, he installed pressure sensors in the spiral casing area and verified the pressure field parameters. Chen et al. stated in their paper [6] that a number of authors dealing with the issue of internal pump flow routinely verified the results of their numerical models using the PIV (Particle Image Velocimetry) method. Another important research area involves studies focusing on the flow in the suction pipe, specifically the effect of the inducer [7] and the Inlet Guide Vane (IGV). The issue of flow modification in the suction pipe using IGV was addressed by Hou et al. [8] They reported in their study that an IGV with six blades had a positive effect on the pump total head, and that a higher number of blades (7 or 9) had a positive effect on the efficiency. The effect of IGV setting angle on the discharge head, efficiency, and cavitation characteristics of centrifugal pump was also discussed by Tan, L et al. [9]. In their work, they used an IGV with six blades for which the inclination can be adjusted.

However, the validation of numerical models, i.e., their experimental verification, remains an issue. For example, Hassan [10] compared the numerical model of a pump in the Ansys program with experimental measurements when innovating an impeller. Alemi [11] in his work verified the numerical model with available experimental data, and there was good accordance between the model's results and reality. The pressures and flowrates of the flowing fluid can be easily verified using pressure gauges and flowmeters. The measurement is described in ISO 9906 standard [12]. Other, more sophisticated methods for capturing fluid flow courses can be PIV methods [13–15]. PIV methods are usually used successfully to verify Ansys simulations [16]. For example, Furst [17] reached an agreement on the streamline's shapes and the fluid velocity when verifying the mathematical model with the measured values in the test laboratory using PIV. On the other hand, Owida [18] compared PIV and Ansys models, using a transparent pump model and investigating the flow in the plane of the impeller and spiral casing. However, he did not reach an agreement. The reason was the imperfect transparency of the pump during experimental measurements. To obtain reliable results from numerical models, the setting of the density of the computational mesh is one of the most important parameters. A coarse mesh is computationally simpler but can severely skew the results. In contrast, a finer mesh gives more accurate results, but the computation time increases, and convergence becomes complicated [2]. It is therefore necessary to check and adjust the computing mesh to ensure its quality. This can be performed, for example, using the Mesh Metric tool. Authors using this tool then evaluate the quality of the computational mesh in their work through the parameters Skewness, Aspect Ratio, or Mesh Quality [19–21].

The aim of this research was to verify the reliability of the numerical Ansys model for predicting fluid behaviour when flowing through a single-stage radial centrifugal pump and to map the flow in the suction pipe.

2. Materials and Methods

Verification tests were conducted on a hydraulic circuit in the Laboratory of Fluid Mechanics at the Faculty of Engineering, Czech University of Life Sciences Prague. A single-stage radial centrifugal cast iron pump with a spiral casing was used for the measurement. The best efficiency point parameters of the pump at shaft speed 1450 min^{-1} are as follows: flowrate Q = 3.54 l/s; total head H = 5.85 m; and efficiency η = 0.63. The evaluation tests were based on the CSN EN ISO 9906 standard, providing the test methods for hydrodynamic pumps.

The test circuit consisted of the tested pump (P), a reservoir with pipes, and control and measuring devices (see Figure 1). The motor with the momentum sensor (D) Magtrol TMB 307/41 (accuracy 0.1%) allowed for the continuous regulation of shaft speed via the frequency converter LSLV0055s100-4EOFNS. The water flow was measured using an electromagnetic flowmeter SITRANS FM MAG 5100 W (accuracy 0.5%). The pressures at the pump inlet (p_s) and the pump outlet (p_p) were measured by the pressure sensor HEIM 3340 (accuracy 0.5%), which was installed according to the first-class accuracy requirements. The power parameters of the pump were measured at constant speed, and velocity field measurement was performed synchronously using the PIV method. The measured pressure values were processed in a way that for each characteristic point the arithmetic mean of the three measured values and their corresponding standard deviations were determine. The standard deviations of the pressures ranged in most cases from 1.6% to 4%. The exception is point 5 (zero pump flow), where the deviation reached 8%. At the optimum pump operation, the standard deviation was minimal, i.e., 1.6%. The efficiency values were processed in the same way and they formed the performance characteristics in Figures 7 and 9. The standard deviations of the efficiency were in the same range as for the pressures and are represented by error bars in the graphs.

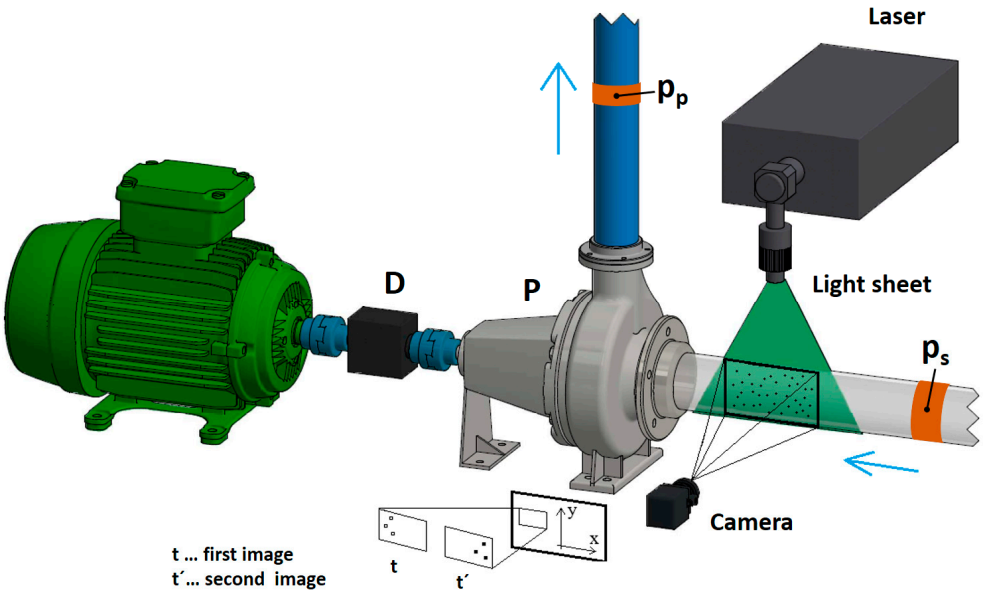

Figure 1. Diagram of setting for pump testing.

A 2D PIV set by TSI company was used to analyse the velocity fields in the pump suction pipe. The basis was a two-pulse Nd:YAG laser (YAG100-100-LIT) with a wavelength of 532 nm, operating with an optical device Light Sheet Optics 610,026, and a camera (Powerview Cameras 630,092). The Modular 610,026 light sheet optics have the capability to allow continuously adjustable focal length between 300 mm to 4000 mm, generating a uniform beam thickness from the laser. The light sheet optics can handle high power laser beams up to 500 mJ, with beam diameter of up to 9 mm. The cylindrical lens diverges the incident laser beam in one direction, creating a flat sheet of light. The divergence is controlled by the focal length of the lens (i.e., the shorter the focal length, the faster the sheet diverges). TSI PowerView Plus 4MP-HS Camera is a multi-bit, 4-megapixel, digital CCD camera. It offers a 2048 × 2048 pixel resolution with a pixel size of 7.4 µm × 7.4 µm, operates at 32 frames per second, and provides a 12-bit output. The set was completed by a synchronizer LaserPulse Model 610,036 and COMPUTER for PIV 600054-64 with INSIGHT™ 4G-2DTR Data Acquisition software. Fluorescent seed particles were dispersed in the flowing fluid—hollow glass spheres 100-SLVR with a diameter of 12 µm, silver-coated to increase the reflection of light on the surface. The density of the seed particles is 1700 kg·m^{-3}.

A vertical plane in the axis of the transparent suction pipe at the pump inlet was selected for monitoring the flow (Figures 2 and 6). A laser was placed above the pipe, repeatedly emitting two consecutive light pulses with a time delay of 50 µs. The optical system directed the emitting laser beam into a thin light sheet which illuminated the monitored area in the suction pipe. Thickness of the light sheet is 0.6 mm. A high-speed camera positioned perpendicular to the plane scanned the area at the same frequency as the laser pulses. This was ensured by the synchronizer. The images from the camera captured the positions of the fluorescent particles. The first image (t) displayed the initial positions of the particles, and the second image (t') the final positions (Figure 1). The image processing was carried out by specialized software, which, by comparing the corresponding pairs, determined the directions and sizes of the velocity vectors of individual particles or flowing fluid. The Scilab program was then used to visualize the measured data. The graphical form of the vector fields was created in this program.

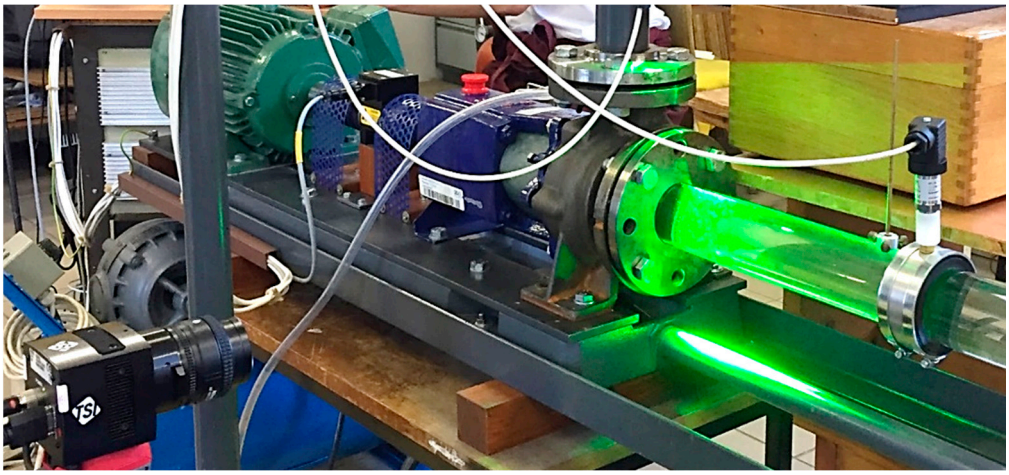

Figure 2. PIV method application during the experiment [22].

Numerical Model of the Flow in the Suction Pipe

Fluid flow can be described in a general way using the Navier–Stokes equations. For the practical solution of pump flow, the equations in their basic form are unsuitable. For their application to issues of flow machines, it is necessary to express them in such a way that the problems associated with momentum transfer and energy dissipation in rotating channels can be solved. For this reason, the Navier–Stokes equations in cylindrical coordinates are used [23,24].

The problem is that the equations express the relationships between the instantaneous values of the velocity or other quantities of the flow field. At the same time, the flow in a hydrodynamic pump is characterized by high values of the Reynolds number and is thus highly turbulent. The instantaneous values of the flow field quantities change with a very high frequency. For these reasons, the structure of the flow field is complicated. In principle, it can be characterised by the formation of flow structures such as eddies and voids. Moreover, these structures are temporally and spatially unstable and their formation, development, and disappearance take place with a high frequency. The aim of CFD simulation is to perform a precise calculation of the flow field quantities, of which the real current field structure is an external manifestation [24].

$$\frac{\partial u_i}{\partial t} + \frac{\partial(\rho u_i)}{\partial x_j} = 0 \tag{1}$$

or rather

$$\frac{\partial(\rho u_i)}{\partial t} + \frac{\partial(\rho u_i u_j)}{\partial x_j} = -\frac{\partial p}{\partial x_i} + \frac{\partial \tau_{i,j}}{\partial x_j} + f_i \tag{2}$$

where ρ is the density; t is the time; u is the velocity; p is the static pressure; τ is the stress tensor; and f is the volume force that includes the Coriolis force and the centrifugal force [25].

At present, the standard k–ε model is the most basic of the double equations model, the most widely used being the eddy viscosity model [24,26]. The equations are as follows:

turbulence kinetic energy k,

$$\frac{\partial(\rho k)}{\partial t} + \frac{\partial(\rho k\, u_i)}{\partial x_i} = \frac{\partial}{\partial x_j}\left[\left(\mu + \frac{\mu_t}{\sigma_\varepsilon}\right)\frac{\partial k}{\partial x_j}\right] + G_k - \rho\varepsilon - S_k \tag{3}$$

dissipation rate ε,

$$\frac{\partial(\rho \varepsilon)}{\partial t} + \frac{\partial(\rho \varepsilon\, u_i)}{\partial x_i} = \frac{\partial}{\partial x_j}\left[\left(\mu + \frac{\mu_t}{\sigma_\varepsilon}\right)\frac{\partial \varepsilon}{\partial x_j}\right] + C_{1\varepsilon}\frac{\varepsilon}{k}G_k - C_{2\varepsilon}\rho\frac{\varepsilon^2}{k} + S_\varepsilon \tag{4}$$

where μ_t is the turbulent dynamic viscosity,

$$\mu_t = \rho C_\mu \frac{k^2}{\varepsilon} \tag{5}$$

G_k is the turbulent kinetic energy,

$$G_k = \mu_T \left(\frac{\partial u_i}{\partial x_j} + \frac{\partial u_j}{\partial x_i} \right) \frac{\partial u_i}{\partial x_j} \tag{6}$$

S_k is the vicious stress, $S_k = 1.0$; S_ε is the turbulence stress, $S_\varepsilon = 1.3$; $C_\mu = 0.09$; $C_{1\varepsilon} = 1.44$; $C_{2\varepsilon} = 1.92$. The numerical values of these quantities correspond to a Newtonian liquid with a viscosity of 1 $m^2 \cdot s^{-1}$ and a density of 1000 $kg \cdot m^{-3}$. Due to the optimal results, their values are used for standard settings of numerical models of water flow through a pump.

The model of the investigated pump (spiral casing, impeller, and suction pipe) was created in the Inventor 2022 program. For the purpose of numerical flow simulations in the Ansys program, a tetrahedron mesh model with different element sizes was created. For the CFD calculation in the CFX module, Element Size: 3 mm and Growth Rate: 1.2 were selected in the global mesh settings. Body Sizing with a mesh density of 4.2 mm was applied to the body of the spiral box (see Figure 3(A)). Inflation (Figure 3(B)) was applied to the surface of the spiral box set to 4 layers with Transition Ratio: 0.45 mm and Growth Rate: 1.3. Using Body Sizing, the impeller mesh was set to Element Size: 2 mm. Inflation (Figure 3(B)) set to 5 layers with Transition Ratio: 0.3 mm and Growth Rate: 1.3 was applied to the surface of the inlet suction pipe. Mesh refinement (Figure 3(C)) was applied to the surface of the radial blade, the shaft end, and the area in between them. The mesh of the inner profile of the inlet suction pipe had global setting parameters (Figure 3(D)).

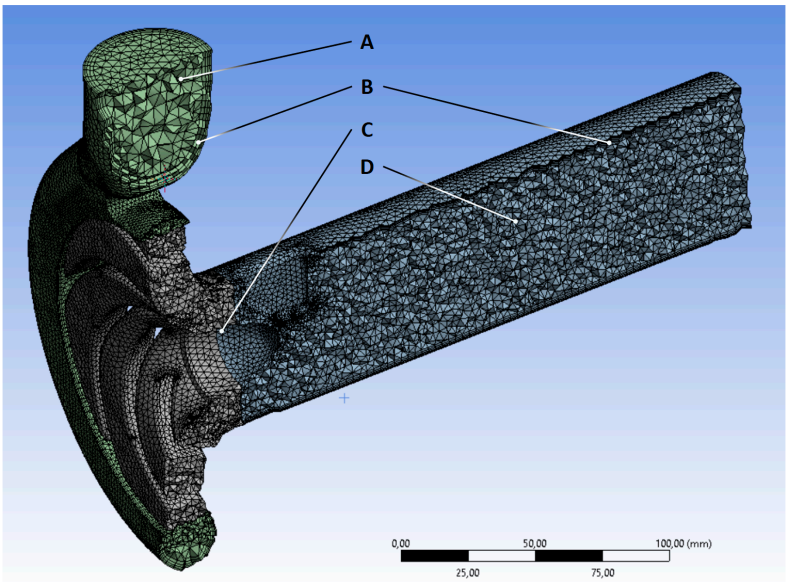

Figure 3. Mesh structure of the computational model. (A)—coarse mesh, (B)—inflation, (C)—fine mesh, (D)—mesh with global setting.

Two of the most important mesh quality parameters are Element Quality and Skewness. The value of Element Quality ranges from 0 to 1. A value of 1 indicates a perfect cube or square, whereas a value of 0 indicates that the element has a zero or negative volume. Its value is determined according to equation:

$$EQ = C \left[V / \sqrt{\left(\sum L^2 \right)^3} \right] \tag{7}$$

where *EQ* is element quality, *V* is element volume, *L* is length of element edge. Parameter *C* corresponds to the element type. For tetrahedrons, *C* = 124.70765802. The frequency of mesh elements was highest in the interval of element quality values from 0.8 to 1 inclusive. Skewness is actually directly related to the quality of mesh structure, and it shows how close the mesh structure is to its ideal shape or form. When the skewness decreases, it means a higher element quality. Figure 4 presents the graphical dependence of the number of elements and its shapes on the skewness value and, at the same time, the skewness quality spectrum [27]. There are tetrahedron, wedge, and pyramid types of elements used in this case, which are the most common for fluid modelling. The numerical model of the pump experimentally verified in this study had the majority of mesh elements in the range of skewness value 0–0.5, which corresponds to very good mesh quality. For the purpose of our modelling, the priority was to achieve the best possible agreement between the model results and the experimentally measured data. For this case, the pressures at the pump inlet and outlet were taken as a comparison criterion. After many experiments with the ANSYS setup, it turned out that the best match is achieved with the meshes the parameters of which are presented in Figure 4.

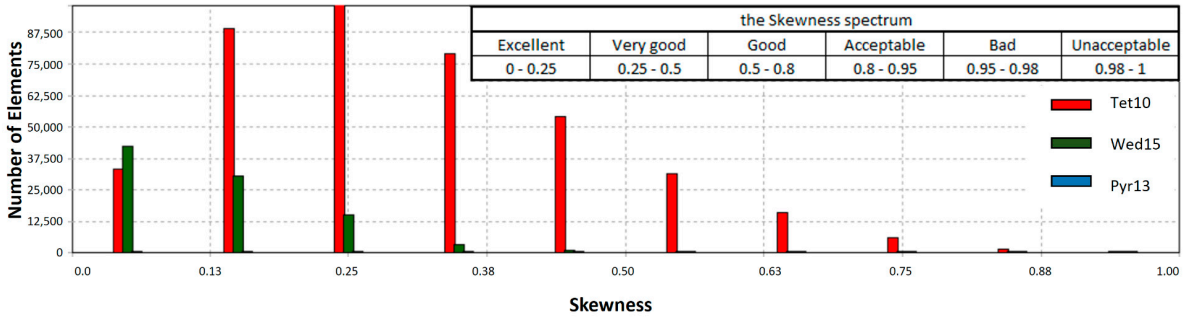

Figure 4. Mesh quality according to skewness.

To validate numerical models of flow using the PIV method, three sets of simulations were created in Ansys, which differ from each other by input parameters. The sets are marked with numbers 1 to 3, and their overview is presented in Table 1. For the first set of simulations, the measured pressure at the pump inlet and the mass flowrate at the pump outlet were used as input parameters. For the second set, the flowrate at the pump inlet and the pressure at the pump outlet were used. For the third set of simulations, the velocity at the pump inlet obtained from the PIV measurement and the flowrate at the outlet were chosen. The calculated values of pressures and flowrates at the control points (P1 to P5) and graphically represented curves of the streamlines in the vertical plane in the axis of the suction pipe were the results of the numerical models (see Figures 5 and 7). Simulations were carried out at all points of the pump performance characteristics.

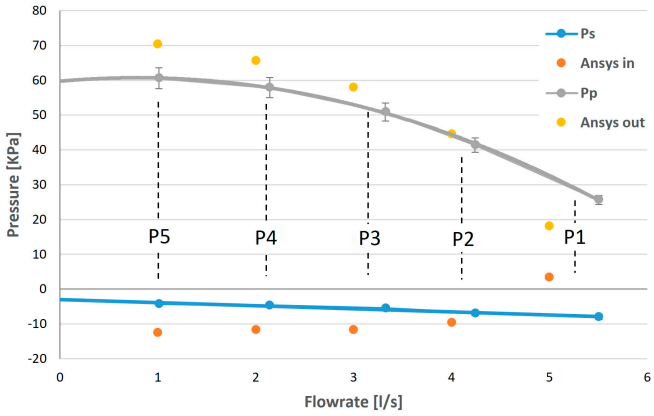

Figure 5. Graph of measured and calculated pressures.

Table 1. Setting input parameters of numerical simulations.

Setting No.	Input Variables for Numerical Model
1	Pressure at the pump inlet, mass flowrate at the pump outlet
2	Mass flowrate at the pump inlet, pressure at the pump outlet
3	Velocity at the pump inlet from PIV, mass flowrate at the pump outlet

3. Results and Discussion

3.1. Pressure Relations in the Pump

The curves in the graph in Figure 5 represent the pressure values (p_s and p_p), including the standard deviation, measured on the test circuit. The measurement of the pump performance characteristic consisted of five partial measurements (P1 to P5). The points in the graph "Ansys out" indicate the CFD calculated outlet pressures at setting 1 and are used for comparison with the measured outlet pressures (p_p). The points "Ansys in" are the calculated inlet pressures at setting 2 and are used for comparison with the measured values of inlet pressures (p_s). Graphical output showing the pressure distributions in the impeller and spiral box are given at the end of this chapter in Figure 9.

At setting 1, the calculated pressure values were very close to the measured values—the largest deviation was 9.8%, the smallest less than 1%. At setting 2, the trend of the pressure course in Ansys was opposite to that of the measured values—i.e., the pressure at the pump inlet gradually decreased while the measured values increased. In most cases, the calculated pressure was significantly lower than the measured pressure, even twice as much. For the calculations applied, that the computation time of the numerical simulations increased with increasing head. In the first control point (P1), the convergence occurred within 500 iterations; in the last (P5), the convergence occurred after 5000 iterations. This behaviour corresponded to the assumptions made by Gülich [2] according to which the unsteady flow tends to converge less easily. In setting 3, the calculation did not converge. Although this setting gave a good agreement with the shapes of the streamlines that corresponded to the PIV measurement, the results cannot be considered. For the reasons mentioned above, setting 1 was used for further simulations and all results presented below were obtained using this setting. The deviation between model and reality is the highest at point 5. This is a situation where the throttle valve on the pump discharge is completely closed and the fluid circulates only between the suction pipe and the impeller. Due to the high degree of difficult-to-predict fluid circulations, it is not easy for ANSYS to model and evaluate these conditions correctly. For this reason, the deviation between calculation and reality is the highest. However, considering that this is an extreme state of the pump operating characteristics, the impact of this deviation on the overall results is only minimal.

3.2. Velocity Profiles in the Suction Pipe of the Pump

Another output of the numerical models in Ansys were vector maps of fluid velocities in the suction pipe of the pump, which were compared with PIV measurements. For these purposes, vector maps were generated in Ansys in the vertical plane identical to PIV measurements. A diagram of the location of monitored profiles in the suction pipe is shown in Figure 6.

Figure 7 shows a summary of both outputs—PIV and Ansys. In the lower-left corner is the performance characteristic of the dependence of the pump efficiency on the flowrate measured during the experiment (P1 to P5). At these points, PIV images were also acquired, and subsequently, numerical simulations in Ansys were performed. To compare the outputs, a pair of images of the fluid velocity fields in the suction pipe before entering the impeller was created for each point of the characteristic. Only at the P3 point was the complete PIV measurement data not available. For this reason, the images are not included here. The fluid in the pipe flows from right to left. The velocity vectors vary in colour according to their size. The highest velocities are depicted in red, and the lowest in blue. The scales of the vectors vary slightly from image to image, so they are not given in the figures for

better clarity. The first pair of images at P1 corresponds to the fully open throttle valve, i.e., the highest flowrate. Here we can observe a steady flow throughout the suction pipe profile. The highest velocities are in the middle section and the lowest near the sides, as is consistent with all assumptions. However, a more gradual decrease in velocity was observed in the upper half of the pipe than in the lower half. This fact is evident in the P2 images, where the agreement between the numerical model and the PIV measurements is more pronounced. The non-uniform velocity distribution is probably caused by the casing rib located in the suction inlet of the pump (see Figure 6). Its function is to direct the fluid in accordance with the assumption of vortex-free entry into the impeller.

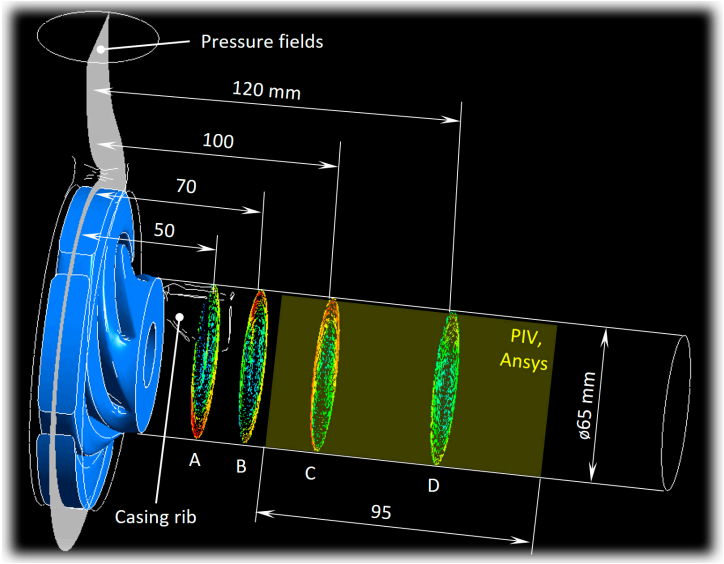

Figure 6. Location of monitored profiles (A, B, C, D—cross-sections depicted in Figure 8).

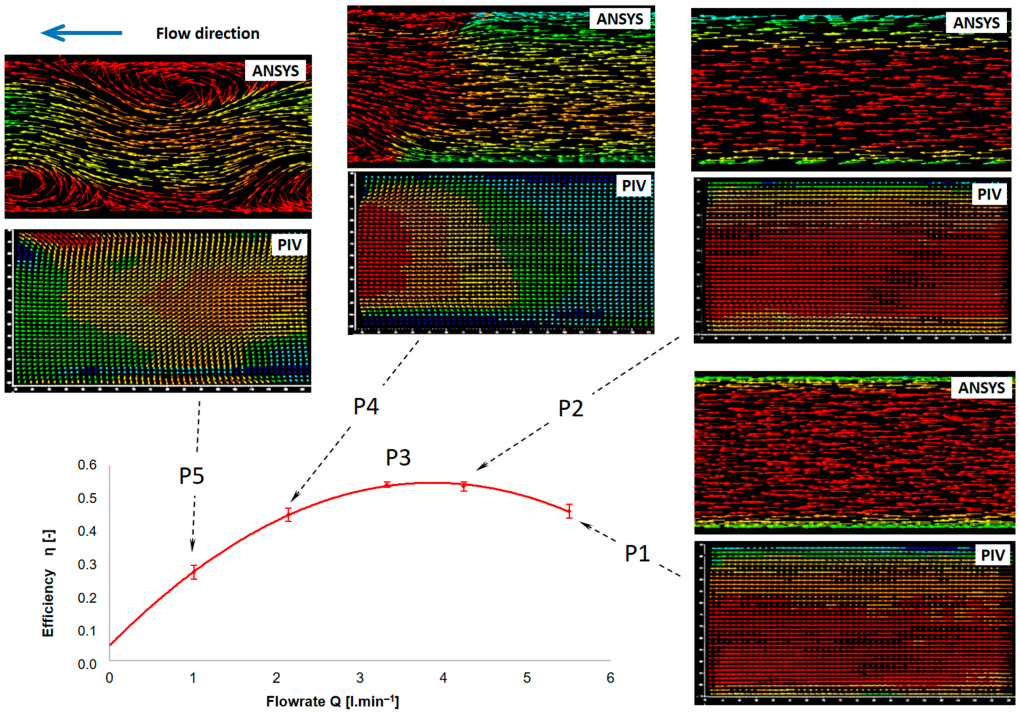

Figure 7. Comparison of vector maps from the numeric model (Ansys, setting 1) and the experiment (PIV).

As the flowrate decreases (point P4), the mean velocity in the pipe also decreases. Due to impeller rotation and viscosity, the fluid accelerates in the middle part of the cross-section, immediately before the pump inlet. Further reduction in the flowrate leads to the formation of local vortices in the pipe and recirculation of the liquid at the pump inlet [2]. This fact is also indicated by the images of radial flow cross-sections created in Ansys for point P5 (see Figure 8), where significantly higher flow velocities can be observed near the sides compared to the middle part of the pipe. However, a 3D PIV measurement would be needed to accurately describe the vortex formation because the particles in this part of the pipe move generally in space and thus outside the monitored plane, which is not captured by the 2D PIV method.

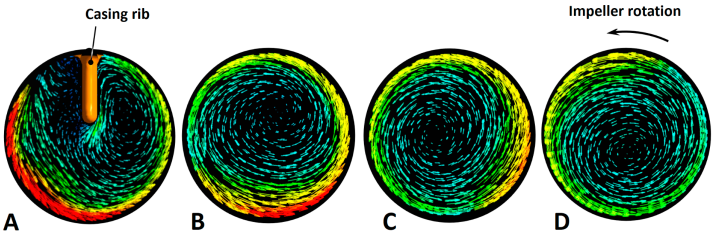

Figure 8. Velocity fields in radial cross-sections of the suction pipe for P5 (Ansys, setting 1). Location of profiles (**A**–**D**) depicted in Figure 6.

In addition to the above velocity fields, the courses of fluid pressure distributions in the impeller and spiral casing were also modelled in Ansys. Individual images of the radial cross-sections are shown in Figure 9, again in relation to the performance characteristic, namely the efficiency course. The scale of pressures is the same for all images and is indicated in the figure. In the images, we can again observe from right to left how the reduction of flow by closing the throttle valve influences the pump discharge. The impeller inlet pressure was measured as part of the performance tests (p_s) and was then used as input value for the pressure field model below. The numerical values of the outlet pressure correspond to the calculation at setting 1 and are presented in Table 1 as "Ansys out". The pressure rise course in the impeller inter-blade spaces corresponds to the theoretical course in an impeller with a finite number of blades, i.e., a more gradual pressure rise on the suction side of the impeller [24].

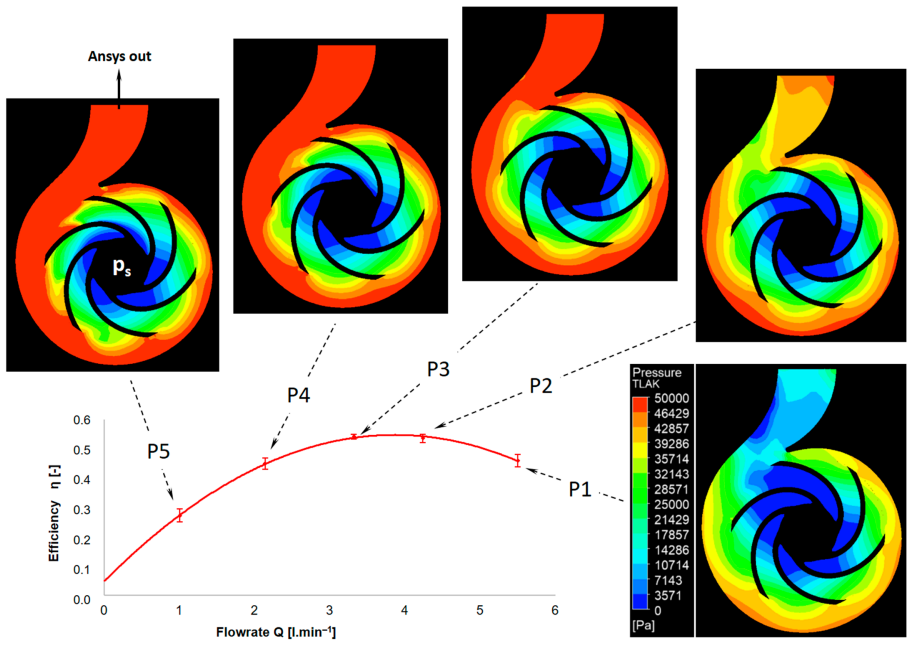

Figure 9. Pressure fields in the impeller and spiral casing (Ansys, setting 1).

4. Conclusions

This research aimed to determine with what reliability it is possible to use a numerical model in Ansys to predict the behaviour of a fluid flowing through a radial centrifugal pump. For this purpose, the model's numerical and graphical outputs were compared with the values of measured performance characteristics and velocity fields obtained from the PIV method. A comparison of the three different model setup methods in Ansys proved the best agreement of the calculation with reality when the pump inlet pressure and the pump outlet mass flowrate were set as input variables (setting 1). In this case, the calculated and measured parameters differed from 1% to 9.8%. If the mass flowrate at the pump inlet and the pressure at the pump outlet (setting 2) were set as input variables, the deviations from reality were much larger. When the velocity at the pump inlet and the mass flowrate at the pump outlet were set as input variables, the calculation did not converge at all. In terms of the analysis of vector maps of the fluid velocities in the pump´s suction pipe, the model presented comparable shapes of streamlines at settings 1. The vector maps from Ansys corresponded well to the outputs from the PIV measurements. Possible differences were caused by the fact that 2D PIV shows vectors projected only into the measured area. Therefore, particles moving in the direction from/to the monitored plane are not displayed in the results. In contrast, the Ansys model can display not only vectors in the area but also their projections into all streamlines in any cross-section of the pipe. The results of this research, together with the Ansys flow model, will be used as a basis for more detailed flow analysis in terms of the anticipated innovations of the radial centrifugal pump.

Author Contributions: Conceptualization, J.Č. and M.P.; methodology, J.Č. and M.P.; software, J.Č. and M.P.; validation, J.Č. and M.P.; formal analysis, J.Č. and M.P.; investigation, J.Č. and M.P.; resources, J.Č. and M.P.; data curation, J.Č. and M.P.; writing—original draft preparation, J.Č. and M.P.; writing—review and editing, J.Č. and M.P.; visualization, J.Č. and M.P.; supervision, J.Č. and M.P.; project administration, J.Č. and M.P.; funding acquisition, J.Č. and M.P. All authors have read and agreed to the published version of the manuscript.

Funding: This study was supported by the Internal grant agency 2022 of the Czech University of Life Sciences Prague, number: 2022:31130/1312/3102.

Data Availability Statement: All data generated or analysed during this study are included in this published article.

Conflicts of Interest: The authors declare no conflict of interest.

References

1. Chandrasekaran, M.; Santhanam, V.; Venkateshwaran, N. Impeller Design and CFD Analysis of Fluid Flow in Rotodynamic Pumps. *Mater. Today-Proc.* **2021**, *37*, 2153–2157. [CrossRef]
2. Gülich, J.F. *Centrifugal Pumps*; Springer: Berlin/Heidelberg, Germany, 2010; Volume c2010, ISBN 978-3-642-12823-3.
3. Polák, M. Innovation of Pump as Turbine According to Calculation Model for Francis Turbine Design. *Energies* **2021**, *14*, 2698. [CrossRef]
4. Sankar, S. Analysis of Centrifugal Pump Impeller Using ANSYS. *Int. J. Innov. Res. Sci. Eng. Technol.* **2018**, *7*, 5021–5026.
5. Meng, D.; Jiang, T.; Deng, H.; Hou, G. Numerical Simulation Research on Radial Force of Centrifugal Pump with Guide Vanes. *Shock. Vib.* **2021**, *2021*, 6638123. [CrossRef]
6. Chen, B.; Qian, Y. Effects of Blade Suction Side Modification on Internal Flow Characteristics and Hydraulic Performance in a PIV Experimental Centrifugal Pump. *Processes* **2022**, *10*, 2479. [CrossRef]
7. Xu, Z.; Kong, F.; Zhang, H.; Zhang, K.; Wang, J.; Qiu, N. Research on Visualization of Inducer Cavitation of High-Speed Centrifugal Pump in Low Flow Conditions. *J. Mar. Sci. Eng.* **2021**, *9*, 1240. [CrossRef]
8. Hou, H.; Zhang, Y.; Li, Z.; Zhang, Y. A CFD Study of IGV Vane Number on Hydraulic Characteristics and Pressure Pulsation of an Is Centrifugal Pump. *J. Vibroengineering* **2017**, *19*, 563–576. [CrossRef]
9. Tan, L.; Cao, S.; Wang, Y.; Wang, B. Influence of Prewhirl Regulation by Inlet Guide Vanes on Cavitation Performance of a Centrifugal Pump. *Energies* **2014**, *7*, 1050–1065. [CrossRef]
10. Hassan, A.; Abdallah, H.; Abou El-Azm Aly, A. Effect of Impeller Blade Slot on Centrifugal Pump Performance. *Glob. J. Res. Eng.* **2016**, *16*, 71–85. [CrossRef]
11. Alemi, H.; Nourbakhsh, S.; Raisee Dehkordi, M.; Najafi, A. Effects of Volute Curvature on Performance of a Low Specific-Speed Centrifugal Pump at Design and Off-Design Conditions. *J. Turbomach.* **2015**, *137*, 041009. [CrossRef]

12. *ISO 9906:2012*; Rotodynamic Pumps—Hydraulic Performance Acceptance Tests—Grades 1, 2 and 3. International Organization for Standardization: Geneva, Switzerland, 2012.
13. Corpetti, T.; Heitz, D.; Arroyo, G.; Memin, E.; Santa-Cruz, A. Fluid Experimental Flow Estimation Based on an Optical-Flow Scheme. *Exp. Fluids* **2006**, *40*, 80–97. [CrossRef]
14. Pedersen, N.; Larsen, P.S.; Jacobsen, C.B. Flow in a Centrifugal Pump Impeller at Design and Off-Design Conditions—Part I: Particle Image Velocimetry (PIV) and Laser Doppler Velocimetry (LDV) Measurements. *J. Fluids Eng.* **2003**, *125*, 61–72. [CrossRef]
15. Feng, J.; Benra, F.-K.; Dohmen, H.J. Unsteady Flow Visualization at Part-Load Conditions of a Radial Diffuser Pump: By PIV and CFD. *J. Vis.* **2009**, *12*, 65–72. [CrossRef]
16. Westra, R.W.; Broersma, L.; van Andel, K.; Kruyt, N.P. PIV Measurements and CFD Computations of Secondary Flow in a Centrifugal Pump Impeller. *J. Fluids Eng.* **2010**, *132*, 061104. [CrossRef]
17. Furst, J.; Halada, T.; Sedlar, M.; Kratky, T.; Prochazka, P.; Komarek, M. Numerical Analysis of Flow Phenomena in Discharge Object with Siphon Using Lattice Boltzmann Method and CFD. *Mathematics* **2021**, *9*, 1734. [CrossRef]
18. Owida, A.; Do, H.; Yang, W.; Morsi, Y.S. Piv measurements and numerical validation of end-to-side anastomosis. *J. Mech. Med. Biol.* **2010**, *10*, 123–138. [CrossRef]
19. Zhou, S.; Lin, P.; Zhang, W.; Zhu, Z. Evolution Characteristics of Separated Vortices and Near-Wall Flow in a Centrifugal Impeller in an Off-Designed Condition. *Appl. Sci.* **2020**, *10*, 8209. [CrossRef]
20. Kumar, J.; Paswan, M. Parametric Analysis of Centrifugal Pump and Calculation of Slip Factor. *Int. J. Sci. Res. Multidiscip. Stud.* **2019**, *5*, 15–22.
21. Ye, F.; Bianchi, G.; Rane, S.; Tassou, S.; Deng, J. Analytical Grid Generation and Numerical Assessment of Tip Leakage Flows in Sliding Vane Rotary Machines. *Adv. Eng. Softw.* **2021**, *159*, 103030. [CrossRef]
22. Černý, J.; Sitte, D. Analysis of the Flow of Liquid in the Suction Pipe of the Radial Centrifugal Pump. In Proceedings of the 22nd International Conference of Young Scientists 2020, Prague, Czech Republic, 14–15 September 2020; Czech University of Life Sciences Prague: Prague, Czech Republic, 2020; Volume 22.
23. Benavides-Morán, A.; Rodríguez-Jaime, L.; Laín, S. Numerical Investigation of the Performance, Hydrodynamics, and Free-Surface Effects in Unsteady Flow of a Horizontal Axis Hydrokinetic Turbine. *Processes* **2022**, *10*, 69. [CrossRef]
24. Varchola, M. *Hydraulický Návrh Odstredivých Čerpadiel*; STU: Bratislava, Slovakia, 2016; ISBN 978-80-8106-070-0.
25. Cao, Z.; Deng, J.; Zhao, L.; Lu, L. Numerical Research of Pump-as-Turbine Performance with Synergy Analysis. *Processes* **2021**, *9*, 1031. [CrossRef]
26. Yang, H.; Zhu, L.; Xue, H.; Duan, J.; Deng, F. A Numerical Analysis of the Effect of Impeller Rounding on Centrifugal Pump as Turbine. *Processes* **2021**, *9*, 1673. [CrossRef]
27. ANSYS. *ANSYS Meshing User's Guide*; Release 14.5 2012; ANSYS, Inc.: Canonsburg, PA, USA, 2012; pp. 124–137.

Disclaimer/Publisher's Note: The statements, opinions and data contained in all publications are solely those of the individual author(s) and contributor(s) and not of MDPI and/or the editor(s). MDPI and/or the editor(s) disclaim responsibility for any injury to people or property resulting from any ideas, methods, instructions or products referred to in the content.